

Component-level Residential Building Material Stock Characterisation Using Computer Vision Techniques

Menglin Dai,^{*,†} Jakub Jurczyk,[‡] Hadi Arbabi,[‡] Ruichang Mao,[¶] Wil Ward,[‡]
Martin Mayfield,[‡] Gang Liu,[†] and Danielle Densley Tingley[‡]

[†]*College of Urban and Environmental Sciences, Peking University, 100871 Beijing, China*

[‡]*Department of Civil and Structural Engineering, The University of Sheffield, Sheffield, S1
3JD, United Kingdom*

[¶]*Department of Environmental and Resource Engineering, Technical University of
Denmark, Kgs Lyngby 2800, Denmark*

E-mail: menglin.dai@pku.edu.cn

Phone: +44 (0)7446885153

1 Abstract

2 The residential building material stock constitutes a significant part of the built
3 environment, providing crucial shelter and habitat services. The hypothesis concerning
4 stock mass and composition has garnered considerable attention over the past decade.
5 While previous research has mainly focused on the spatial analysis of building masses, it
6 often neglects the component-level stock analysis or requires heavy labour cost for onsite
7 survey. This paper presents a novel approach for efficient component-level residential
8 building stock accounting in the UK, utilising drive-by street view images and building
9 footprint data. We assessed four major construction materials: brick, stone, mortar,

10 and glass. Compared to traditional approaches that utilise surveyed material intensity data, the developed method employs automatically extracted physical dimensions
11 of building components incorporating predicted material types to calculate material
12 mass. This not only improves efficiency but also enhances accuracy in managing the
13 heterogeneity of building structures. The results revealed an error rate of 5% and 22%
14 for mortar and glass mass estimations, and 8% and 7% for brick and stone mass esti-
15 mations, with known wall types. These findings represent significant advancements in
16 building material stock characterisation and suggest that our approach has considerable
17 potential for further research and practical applications. Especially, our method estab-
18 lishes a basis for evaluating the potential of component-level material reuse, serving the
19 objectives of a circular economy.

20

21

22 **Keywords:** building material stocks, urban sustainability, circular economy, deep
23 learning, computer vision, building facade, street view imagery

24 **Synopsis:** This study introduces a computer vision-based method for precise component-
25 level quantification of building materials, advancing circular economy efforts.

²⁶ Introduction

²⁷ Residential buildings, integral to human habitation and contributing 62.2% of total building
²⁸ carbon emissions¹, play a pivotal role in the built environment achieving the United Nations'
²⁹ Sustainable Development Goals². These structures rely on construction materials which have
³⁰ formed a major portion of the anthropogenic mass of approximately 1.1 teratonnes, which
³¹ has exceeded living biomass since 2020.^{3,4} Knowledge, e.g. type and quantity, of these mate-
³² rials is crucial to facilitating a circular economy,⁵ aiding in building decarbonisation efforts
³³ by reducing demand for new materials through urban mining⁶ and facilitating related policy-
³⁴ making.⁷ Existing research largely studies the residential building stock from a geographical
³⁵ viewpoint, focusing on spatial analysis of material stock,^{8,9} but often overlooks individual
³⁶ building analysis. This gap warrants further investigation for a more geographically specific,
³⁷ nuanced understanding.

³⁸

³⁹ The state-of-the-art techniques for acquiring building stock information can be aptly clas-
⁴⁰ sified into three distinct approaches:^{8,10,11} top-down, bottom-up, and remote sensing. The
⁴¹ top-down approach involves viewing target objects as a complete system, with the material
⁴² stock being equivalent to the mass balance of inflow and outflow within the system. The
⁴³ utilisation of socioeconomic statistics data is a prevalent practice in the implementation of
⁴⁴ this approach.^{12–15} As a result, it is often employed for material stock simulation at the
⁴⁵ level of a nation due to the data availability.^{8,16} Conversely, the bottom-up approach begins
⁴⁶ at the end-use object inventory stage, where the number of buildings is collated to derive
⁴⁷ the building material stock for a specific time period, with material intensity coefficients
⁴⁸ employed to calculate the material stock.^{17–22} The implemented bottom-up approaches have
⁴⁹ shown their capability of achieving considerably finer resolution than top-down approaches.
⁵⁰ Recently, the application of remote sensing data for material stock accounting has garnered
⁵¹ considerable attention.^{23–25}

⁵²

53 To accurately evaluate building material stock at the individual building-level resolution,
54 component-level understanding of each structure is imperative.^{26,27} Consequently, top-down
55 and satellite image-based remote sensing methods are insufficient for this task. Frequently
56 utilised bottom-up techniques rely on publicly available data for material intensity, neces-
57 sitating meticulous and labour-intensive preparation. In scenarios where no such data is
58 accessible, collaboration with domain experts may prove a feasible alternative, but it is still
59 highly labour intensive.²⁸ An alternative is to develop an automated method for estimating
60 building material stock to facilitate a more efficient procedure.

61

62 Street view imagery serves as a potent data source, encapsulating substantial building-
63 related information with promising utility to estimate building material stock. Over the past
64 decade, navigation companies, notably Google²⁹, have significantly enhanced the availability
65 of such imagery. While previous research has leveraged Street view imagery across various
66 domains³⁰, including specific building attributes such as type³¹, age³², and window-to-wall
67 ratio³³, the application of this data type for comprehensive building stock evaluation remains
68 relatively uncharted and poses distinct challenges.

69

70 One salient challenge is a lack of data containing facade imagery and registered building
71 information. Machine learning techniques, particularly deep learning, offer promising av-
72 enues for building attribute estimation using street view imagery. However, these methods
73 necessitate substantial, diverse, and accurately labelled training data, which presents signif-
74 icant challenges in terms of data collection, annotation, and quality control.

75

76 Another challenge lies in the limited availability of data capture locations; Street View
77 services may not consistently provide frontal, complete views of each building, thus result-
78 ing in partial or oblique images. Moreover, discerning intricate building details necessitates
79 high-resolution imagery. For instance, distinguishing between non-rendered cavity walls and

80 solid brick walls requires the visualisation of brick patterns and, consequently, the discernible
81 mortar joints, typically 1 cm thick in masonry structures. To attain the requisite clarity,
82 imagery should ideally possess a minimum of 1 pixel per centimetre, translating to a 600-
83 pixel image size for a standard two-storey, 6-meter tall building. Nevertheless, the Google
84 Street View API²⁹ currently limits downloadable image size to 640 pixels, which significantly
85 constrains the effective use of this service for detailed analysis.

86

87 This paper presents a novel method that integrates high-quality geo-referenced street view
88 facade images with machine learning-based computer vision techniques to enable component-
89 level building material stock characterisation. The study typically focuses on houses lower
90 than three storeys which make up 94% of UK households.³⁴ This proposed approach fa-
91 cilitates the characterisation of individual buildings by capturing essential features such
92 as component quantity, composition, built form, and age while requiring fewer assump-
93 tions than conventional bottom-up models. To develop this approach, we have compiled
94 a comprehensive dataset of 2,292 houses, enriched with high-resolution facade images and
95 detailed attributes, and created specialised datasets for interior wall length estimation using
96 facade features (300 UK houses) and construction material recognition (13,562 labelled image
97 patches). Additionally, a new building age detection dataset (9,278 images) has been intro-
98 duced, along with an innovative multi-task deep learning model for simultaneous building
99 age and built form recognition.

100 Materials and Methods

101 Workflow Overview

102 Figure 1 illustrates the workflow of the developed approach, which comprises of five individ-
103 ual modules, from data collection to material stock calculation. The data collection process
104 aims to establish a matched facade image & building footprint data. Subsequently, the fa-

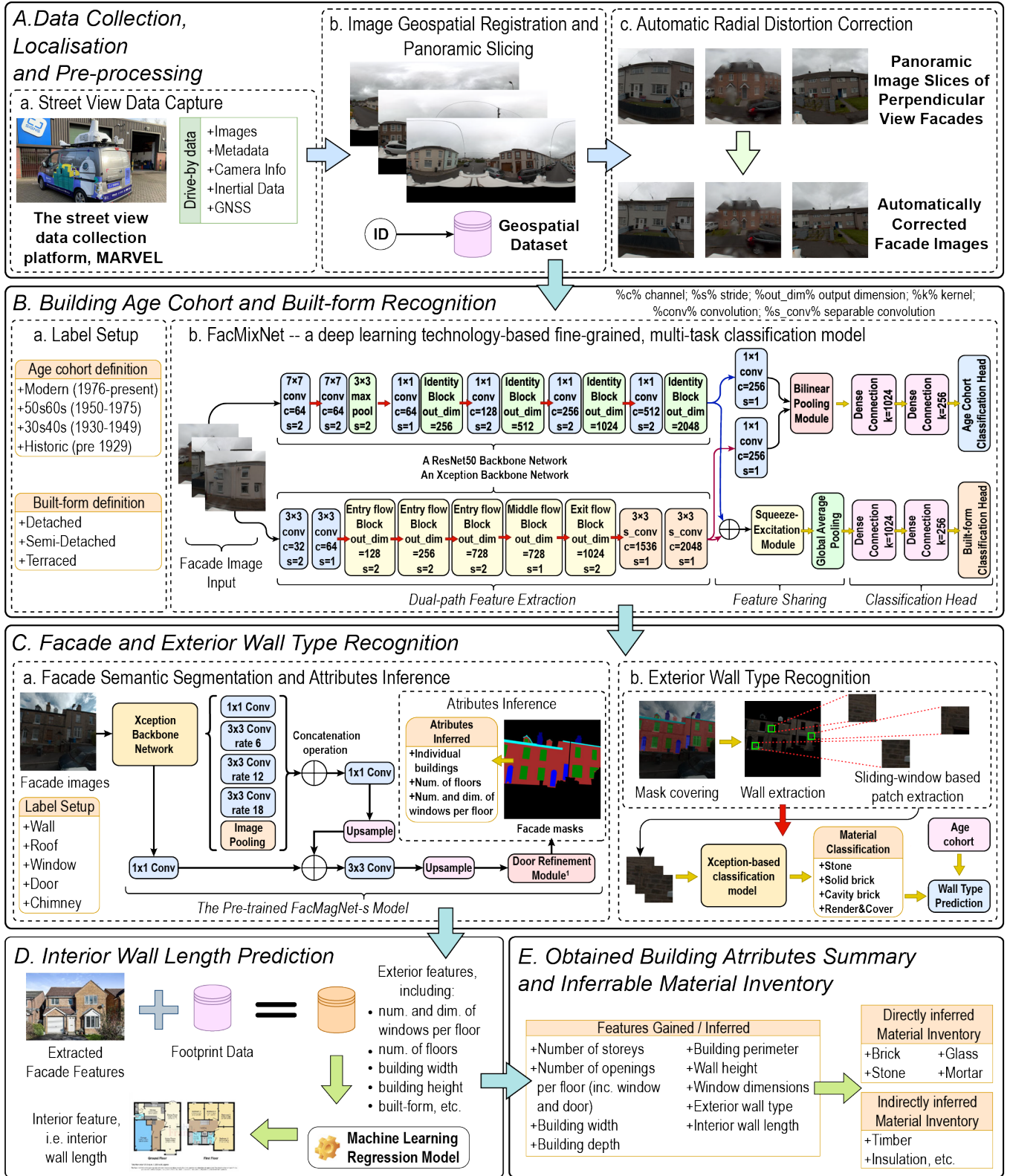
105 facade images are utilised to predict houses' age cohort, built form, i.e., detached, terraced,
106 and semi-detached, and component locations, as illustrated in panels B and C. The predicted
107 facade masks facilitate the estimation of the number of floors and openings i.e. windows and
108 doors per floor. Moreover, the predicted masks are employed to extract patches from wall
109 areas, which are subsequently used to predict the wall material type. The estimated building
110 attributes are then fed into a regression model to predict the inner wall length, followed by
111 the computation of the volume of inner walls. In the final step, all the achieved building
112 attributes are used to calculate the mass of each designated material type.

113

114 Overall, our approach uses visible facade features and publicly available building footprint
115 data to derive an individual house's material stock. The material stock of a given area can
116 then be determined by summing the material stock of all individual buildings. The selected
117 visible features include facade wall type, age, built form, and the spatial distribution of
118 building openings, e.g. windows and doors. Wall type directly correlates to wall materials
119 and in some cases may indicate insulation conditions while building age and built form link
120 to pre-defined archetype databases such as the TABULA dataset³⁶. These databases aid in
121 the estimation of invisible materials such as timber from floor decks and roof structures and
122 insulation. The spatial distribution of windows can be used to estimate the mass of glass. By
123 incorporating dimension information obtained from the building footprint database, the mass
124 of brick, stone, mortar and glass can then be directly obtained. This approach represents a
125 significant contribution to the field of material stock analysis, as it provides a comprehensive
126 and automated workflow for the estimation of building material stock from facade images.

127 Drive-by Data Capture

128 A built vehicle-mounted data capture platform³⁷ was employed to collect street view facade
129 images in this study. The platform contains an advanced multi-camera rig and an onboard
130 inertial measurement unit (IMU) and a global navigation satellite system (GNSS) unit for



¹ Referring to Dai et al. (2021) for the refinement module structure

Figure 1: The developed material stock inventory characterisation pipeline. The data capture platform figure in Panel A-a is adapted from Dai et al. (2022).³⁵

¹³¹ capturing raw image data and synchronised orientation/location data. The camera rig com-
¹³² prises six separate 2/3-inch Sony IMX264 CMOS sensors with 2048×2448 effective pixels
¹³³ and wide-angle lenses with a frequency of 30 frames per second (FPS). The cameras are
¹³⁴ oriented with one on the top pointing upwards and the other five positioned horizontally
¹³⁵ along the sides forming a regular pentagon. The combined capture has a field-of-view of
¹³⁶ 90% of the full sphere.

¹³⁷

¹³⁸ During the data collection process, the capture platform traverses the designated area,
¹³⁹ which for demonstration in this paper is Merthyr Tydfil town, Wales, the UK. The platform
¹⁴⁰ travels at a speed of approximately 4.5 meters per second and captures data with a frequency
¹⁴¹ of 10 FPS, around 12 images for every meter travelled. At a distance of 10 meters from the
¹⁴² sensing vehicle, each pixel in the image is representative of an area of approximately 2.5 cm^2
¹⁴³ on the target surface which exceeds the 1cm per pixel requisite stated previously. The
¹⁴⁴ onboard IMU/GNSS unit provides an orientation accuracy of 0.1° and a location accuracy of
¹⁴⁵ up to 0.1m, which leads to a 0.25m frame position accuracy at the 4.5m/s driving speed. The
¹⁴⁶ position data from the IMU/GNSS unit is recorded in the World Geodetic System (WGS84)
¹⁴⁷ format, consisting of longitude and latitude coordinates. For applications within the UK,
¹⁴⁸ these coordinates are reprojected to the Ordnance Survey National Grid reference system
¹⁴⁹ (OSGB 1936).

¹⁵⁰

¹⁵¹ The previously proposed algorithm, designed to extract perpendicular views of specified
¹⁵² houses and register these with footprint data, is employed to obtain the ‘face-on’ views of the
¹⁵³ designated houses^{38,39}. The method first reconstructs the panoramic image using frames from
¹⁵⁴ all five sensors and then slices the captured panorama based on vehicle orientations. Then by
¹⁵⁵ adopting the Ordnance Survey topographic identifier (TOID), the extracted perpendicular
¹⁵⁶ view slices are linked to the property footprint data⁴⁰. The extraction of perpendicular-view
¹⁵⁷ facade images from captured panoramas inherently introduces radial distortion. Given that

158 these images are sliced from panoramic views, traditional chessboard-based image rectifica-
159 tion methods⁴¹ prove inapplicable. To address this, an automatic radial distortion correction
160 approach⁴² is implemented on the building-registered images prior to further processing.

161 **Datasets**

162 This section introduces all datasets built or used in this study. More details of these datasets
163 such as annotation protocols, data distributions and comparison studies are available in the
164 supporting information.

165 **The Housing Attributes Dataset** This dataset comprises 2,292 houses, featuring facade
166 images, footprint data, age cohorts, built forms, wall types, and opening information. It
167 is based on the footprint-registered street view facade images obtained through the data
168 collection procedure in Merthyr Tydfil, Wales, the UK. The facade data is then aligned with
169 the UK Energy Performance Certificate (EPC) records,⁴³ employing property identifiers to
170 obtain wall type, building age and built form data. Subsequently, visual wall materials,
171 building dimensions, and opening sizes are manually obtained.

172 **The Age-Built form Dataset** A dataset comprising 9,278 annotated images was con-
173 structed using Google Street View data by following the subsequent steps: Initially, 21,207
174 EPC records were collected. Duplicate and invalid records were filtered out, and the re-
175 maining location data was used to query and download corresponding building images via
176 the Google Street View API. Each downloaded image was manually inspected for address
177 matching, appropriate camera orientation, and suitable resolution, retaining only images
178 with perpendicular views and acceptable resolution. The finalised dataset was randomly
179 divided into training (80%), validation (10%), and test sets (10%).

180

181 The EPC categorises household age cohorts based on energy performance, but direct
182 utilisation of these labels is challenging as narrow age cohorts may result in significant con-

¹⁸³ fusion as shown in previous research.³² This study harmonises EPC age cohort classifications
¹⁸⁴ by integrating the TABULA Building Archetype project³⁶ and the BRE Housing Survey⁴⁴,
¹⁸⁵ resulting in four simplified groups: pre-1930s, 1930-1949, 1950-1975, and 1976-present. Addi-
¹⁸⁶ tionally, built-form labels are streamlined, merging end-terraced and mid-terrace categories
¹⁸⁷ into a single terrace label.

¹⁸⁸ **The Facade Recognition Dataset** The Sheffield Crookesmoor facade recognition dataset
¹⁸⁹ which is fine-labelled for building facade semantic segmentation is adopted in this study.⁴⁵
¹⁹⁰ This dataset consisted of 997 images annotated to five categories: window, door, wall, roof
¹⁹¹ and chimney and specifically focusing on UK housing, and the data was obtained from the
¹⁹² same data capture platform as in this study. The dataset has been randomly split into 80%,
¹⁹³ 10%, and 10% training, validation, and test sets, respectively.

¹⁹⁴ **The Material Patch Dataset** A material patch dataset comprising 13,562 images was
¹⁹⁵ constructed for this study, labelled into four categories: solid brick, cavity brick, stone, and
¹⁹⁶ render. This dataset was created using data from the previous captures with the same data
¹⁹⁷ collection platform as this study.^{35,39,45} The dataset was randomly split using the same ratio
¹⁹⁸ as in previous datasets, i.e., 80% for training, 10% for validation, and 10% for testing.

¹⁹⁹ **The Inner Wall Regression Dataset** The dataset contains 300 houses with floorplans
²⁰⁰ and annotations across the UK. The dataset is sourced from real estate websites Zoopla
²⁰¹ (<https://www.zoopla.co.uk/>) and Savills (<https://www.savills.com/>). Co-authors with
²⁰² architecture expertise are responsible for collecting raw data to ensure its high quality. The
²⁰³ samples were meticulously labelled—visually and through AutoCAD—enabling precise iden-
²⁰⁴ tification and measurement of features, including building types, interior wall length, perime-
²⁰⁵ ters, width, depth and quantities and dimensions of windows and doors.

206 **Building Age Cohort and Built Form Recognition**

207 In recent years, automatic recognition of building ages using facade images has garnered
208 significant attention in the context of deep learning.^{32,39,46,47} Zeppelzauer et al. (2018)³²
209 pioneered a patch-based approach, wherein building images are segmented into patches con-
210 taining potential age-relevant features. These patches are input to a deep learning model,
211 and aggregated predictions inform the building’s age estimate.

212

213 However, this patch-slicing technique, initially designed for fine-grained classification
214 tasks, is non-differentiable and introduces extra computational costs due to its two-stage
215 nature of localisation and classification.⁴⁸ Bilinear pooling, a fully differentiable technique,
216 has emerged as a compelling alternative, achieving comparable performance with reduced
217 computational overhead and enabling end-to-end training.⁴⁹

218

219 The proposed model in this study, named FacMixNet, integrates a shared feature extrac-
220 tion architecture for the dual prediction of building age and built form—two attributes that
221 are conventionally classified separately.^{46,50} The novel multitask learning framework posits
222 the potential interrelation of features used for both age and built form recognition, as de-
223 picted in Figure 1 Panel B.

224

225 FacMixNet adopts a dual-path architecture, using ResNet50⁵¹ and Xception⁵² as distinct
226 backbone networks for feature extraction. For age prediction, a bilinear pooling module fuses
227 features, but given its substantial memory demands, 1×1 convolution kernels are applied to
228 reduce feature map dimensions. In contrast, for built-form prediction, FacMixNet employs
229 a straightforward concatenation operation, premised on the assumption of more distinct
230 feature categories. A channel-wise attention module is introduced post-concatenation to ac-
231 centuate key features.

232

²³³ In summary, this study introduces FacMixNet, a multi-task deep learning model designed
²³⁴ for the dual prediction of building age and built form from facade images. It strategically
²³⁵ employs bilinear pooling and concatenation methods, reflecting the nuanced demands of
²³⁶ these distinct yet related classification tasks, and provides an efficient, streamlined solution
²³⁷ for building attribute recognition. Training details are available in the supplementary file.

²³⁸ Facade Segmentation and Attributes Estimation

²³⁹ Facade semantic segmentation seeks to identify building components, such as windows and
²⁴⁰ doors, in images at the pixel level. While rectified and cropped facade images have been
²⁴¹ prevalent for 3D procedural modelling,^{53,54} recent work has shifted towards using street view
²⁴² images, which are more abundant and preserve building context.^{45,55}

²⁴³

²⁴⁴ Door recognition, a critical aspect of segmentation, remains challenging due to its typi-
²⁴⁵ cally lower intersection-over-union (IOU) metrics compared to overall dataset mean IOU.^{45,55,56}
²⁴⁶ Doors are pivotal for discerning building attributes, such as the number of floors and indi-
²⁴⁷ vidual units in terraced structures.

²⁴⁸

²⁴⁹ In this study, a more efficient version of the previously developed FacMagNet model⁴⁵
²⁵⁰ termed FacMagNet-s is proposed. FacMagNet-s leverages a Deeplabv3+⁵⁷ model as a multi-
²⁵¹ class classifier for predicting all classes. Instead of employing an object detection model to
²⁵² refine predicted components, FacMagNet-s directly utilises the door predictions to calculate
²⁵³ bounding boxes, followed by the previously designed magnifier module. The model structure
²⁵⁴ is shown in Figure 1 Panel C-a and training details are available in the supplementary file.

²⁵⁵

²⁵⁶ To isolate the spatial distribution of facade openings of individual houses, this work
²⁵⁷ presents a pixel intensity-based algorithm. It applies a morphological open operation to a
²⁵⁸ binary facade mask, followed by a vertical pixel intensity projection. This method identifies

259 the primary building structure by detecting the longest span between sharp declines in pixel
260 intensity, effectively excluding neighbouring structures from the analysis. For terraced and
261 semi-detached houses, the location of doors is utilised to extract separate residences.

262

263 In estimating the distribution of windows on facades, we leverage the positions of doors,
264 roofs, and wall trisection lines. The methodology is founded on specific architectural reg-
265 ularities, the details of which are outlined as assumptions in the supplementary file. By
266 incorporating these assumptions, we develop a rule-based algorithm with K-means cluster-
267 ing to estimate the window arrangements in various house types, including terraced, semi-
268 detached, and detached houses. Implementation particulars of this algorithm are detailed in
269 the pseudo-code provided in the supplementary material. Once the vertical distribution of
270 windows is ascertained, the achieved primary building location is then applied to obtain the
271 window distribution of the designated house.

272 Exterior Wall Type Recognition

273 Wall construction types are crucial for estimating material requirements. In the UK, brick
274 is the dominant construction material, with stone also being used. The British Energy Per-
275 formance Certificates (EPCs) categorise walls into four types: cavity walls, solid brick walls,
276 sedimentary rock walls, and igneous rock walls.⁵⁸ Stone and brick walls have distinct visual
277 features, and brick layouts differ between solid and cavity walls.

278

279 A significant challenge is the rendering of outer walls, which can obscure the wall's tex-
280 ture—a key identifying feature—making visual data unreliable as shown in Figure 2. More-
281 over, different materials can be used within the same building for decorative purposes. An
282 Xception model is first trained on the built material recognition dataset. Training details of
283 the Xception model are available in the supplementary file.

284

285 Noting the correlation between wall types and building ages—solid walls in Victorian
286 buildings and cavity walls become prevalent from the 1920s⁵⁹—this study then introduces
287 an age-assisted wall identification approach. This integrates visual characteristics, experi-
288 ential insights, and building age data to overcome the ambiguities introduced by rendering
289 and intra-building material variations, thereby enhancing wall identification accuracy.

290

291 During inference, depicted in Figure 1 Panel C-b, the predicted wall mask is used to
292 extract wall area samples from raw images, which are then analysed by the trained Xception
293 model. Subsequently, we employed a sliding box to randomly sample 50 patches from the
294 wall area. These samples were then fed into the trained Xception model for inference.
295 Acknowledging that diverse materials may be present on a single wall, we propose a material-
296 ranking approach for filtering predictions. In this scheme, solid brick holds the highest
297 priority; rendering wall has the lowest, and cavity brick and stone are of equal priority. For
298 fully rendered buildings constructed post-1929, cavity brick is the default classification. For
299 those built pre-1929, they are classified as solid brick. While buildings with stone features
300 built after the 1930s are still classified as cavity brick.

301 Interior Wall Regression

302 To accurately estimate the material stock, the interior walls play a crucial role and acquiring
303 such information is a tremendous challenge. The interior wall information can be retrieved
304 from architectural layout plans or via onsite surveys. However, the former option is often
305 hampered by severe data scarcity, while the latter is significantly labour-intensive. Mean-
306 while, to calculate the material stock, a detailed floor layout is not necessary but the total
307 length of the inner wall is adequate. With known inner wall length and height from footprint
308 data, the weight of the inner walls can be calculated if we know its material type which has
309 been inferred in the previous section.

310

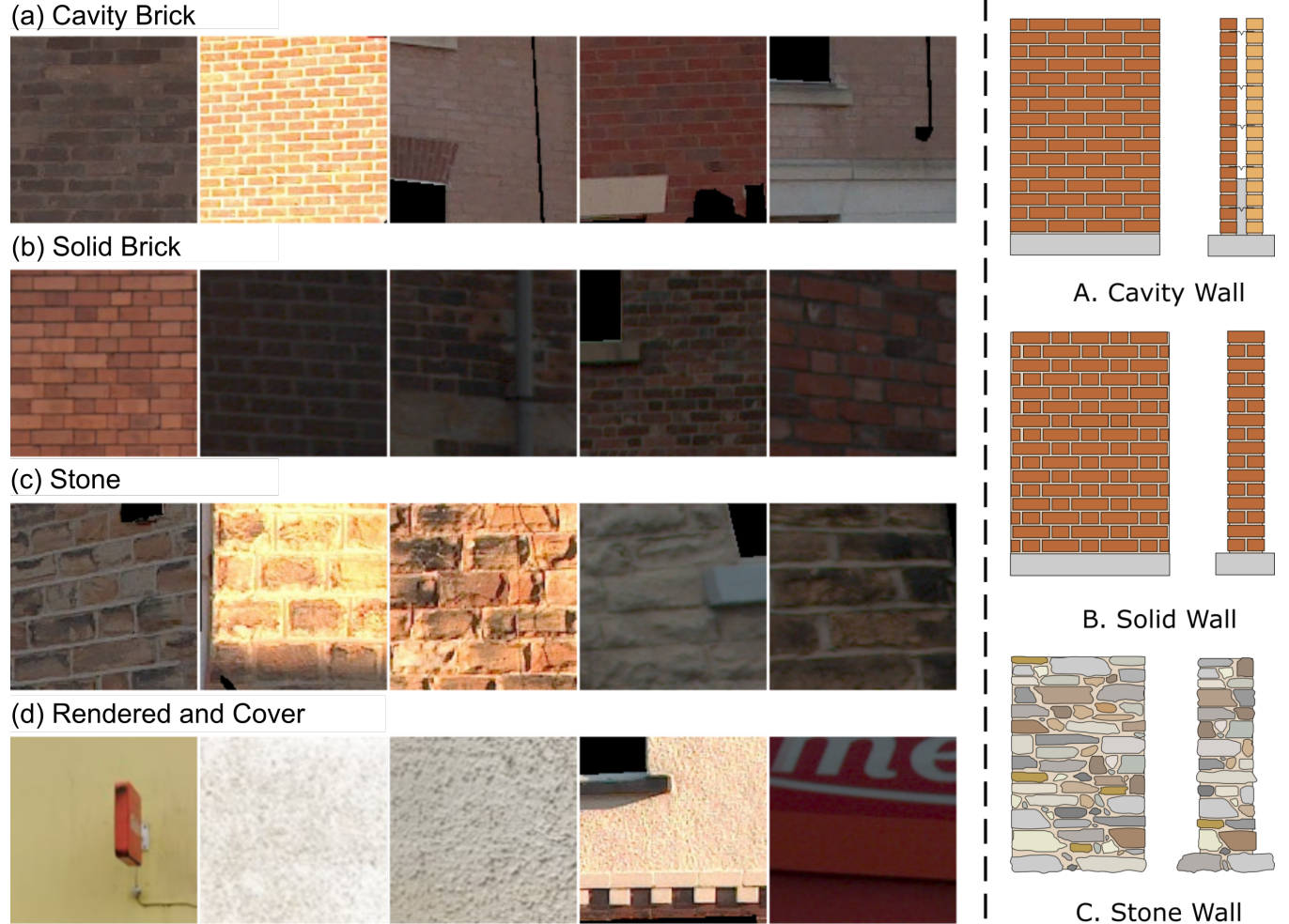


Figure 2: Typical Masonry Wall Patterns and Wall Type Structures. The three wall types are approximated to their archetypal forms: cavity walls consist of two layers of bricks, solid walls exhibit a cross-laid pattern, commonly referred to as Flemish bond, and stone walls are constructed using amorphous shaped stone chunks, which are adhered together using mortar.

311 We posit that there exists a correlation between the total inner wall length of a building
312 and its external features, including windows, building length, building depth, and overall
313 architectural form. Consequently, estimating the inner wall length presents a regression
314 problem. In a similar vein, Yuan et al.⁶⁰ investigated the use of building exterior features to
315 estimate the weight of buildings based on waste management data from Hong Kong. Their
316 study involved the construction of a dataset comprising 78 building samples, utilising mul-
317 tiple data sources. Taking inspiration from their work, we built the inner wall regression
318 dataset. We adhere to the same process as their work for our regression analysis.⁶⁰

319

320 In choosing regression models, the Multi-Layer Perceptron (MLP) is adopted. The model
321 structure is determined using a grid search strategy with the maximum number of hidden
322 layers being 2 and the number of kernels ranging from 5 to 10. The activation function is
323 determined to be Relu and the optimiser is chosen to be Adam. The number of epochs is
324 determined to be 5000 and the early stopping is enabled. The model and evaluation are
325 performed using the Python scikit-learn package.⁶¹

326 Material Stock Estimation

327 As our approach is vision-based, we primarily focus on calculating materials which are visible
328 in a building in this paper including brick which is the major English housing construction
329 material⁶², stone, glass and mortar. By establishing connections between the derived build-
330 ing attributes and supplementary data sources, such as historical construction standards, we
331 can deduce the use of other types of construction materials, including insulation, wood and
332 metals. It is important to note, however, that as this paper serves as a framework, we do
333 not delve into the estimation of the whole material masses at this stage.

334

335 In the UK, bricks typically adhere to a standard size of $215 \times 102.5 \times 65\text{mm}$, while mortar
336 maintains a standard thickness of 10 mm.⁶³ Utilising these dimensions, a double-skin brick

³³⁷ wall, whether a cavity wall or solid brick wall, necessitates an average of 118 bricks per square
³³⁸ meter. Consequently, for a single-skin brick wall, the brick requirement would be reduced to
³³⁹ 59 bricks per square meter. The brick density is assumed to be 2000 kg/m^3 and the mortar
³⁴⁰ density is assumed to be 2300 kg/m^3 .

³⁴¹

³⁴² A notable aspect of this study is the consideration of structural elements in buildings.
³⁴³ First, the exterior walls are all assumed to be load-bearing. Second, when a building's long
³⁴⁴ side exceeds 6 meters, the typical maximum span of a timber structural beam, a calcula-
³⁴⁵ tion is introduced: the building's long side length is divided by 6 meters, and the resulting
³⁴⁶ quotient is multiplied by the building's short side length. This product is then assumed to
³⁴⁷ represent the length of load-bearing walls within the building. Then the rest of the interior
³⁴⁸ walls are assumed to be single-skin brick walls.

³⁴⁹

³⁵⁰ Despite the irregular patterns of stone walls, the approach assumes that stone used for
³⁵¹ construction can be treated similarly to regular bricks for weight calculations. In other ways,
³⁵² the calculation of the stone house is assumed to be the same as the brick houses. The density
³⁵³ of stone is assumed to be 2500 kg/m^3 .

³⁵⁴

³⁵⁵ To estimate glass weight, the resolution of the image is inferred by assuming each floor
³⁵⁶ is 3m tall and obtaining the number of pixels of the wall height in the image. The glass
³⁵⁷ area is then calculated from window dimensions, with an assumption of a 70-millimetre-
³⁵⁸ wide window frame and a 4-millimetre glass thickness. Besides, buildings built after 1970
³⁵⁹ are assumed to be double glazing and otherwise to be single glazing. Using this area, the
³⁶⁰ density of the glass and the assumed glazing type, the weight of the glass is computed.

³⁶¹ **Results and Discussion**

³⁶² **Material Mass Estimation Performance**

³⁶³ Figure 3 demonstrates the prediction performances of the computer vision-driven material
³⁶⁴ stock estimation approach. EPC records and manually measured attributes provide refer-
³⁶⁵ ence values, while the proposed method furnishes predicted values. Each subplot includes a
³⁶⁶ line with a gradient of one, denoting the expectation function, and the mass distributions
³⁶⁷ for reference and prediction are displayed on the top and right margins, respectively.

³⁶⁸

³⁶⁹ The data reveals exemplary performance in mortar mass prediction, with a 5% error rate
³⁷⁰ among the 2,292 samples, evidenced by the close alignment of the fitting function to the
³⁷¹ expectation function.

³⁷²

³⁷³ The prediction of glass mass has achieved the second-best result with an overall error
³⁷⁴ rate of 22%. However, The variance of glass prediction is higher than the mortar.

³⁷⁵

³⁷⁶ Brick and stone mass predictions showcase three distinct clusters. One cluster aligns well
³⁷⁷ with the expectation function, pointing to accurate wall type predictions. The other two
³⁷⁸ clusters, residing along the x and y axes, represent misclassified wall types.

³⁷⁹ **Individual Models' Performances**

³⁸⁰ Figure 4 shows the trained classification models' deployment performances using confusion
³⁸¹ matrices. All confusion matrices have been normalised by dividing their number of true
³⁸² labels. All evaluation measures used in this study, including the confusion matrix and
³⁸³ various evaluation metrics, are detailed in the supporting information.

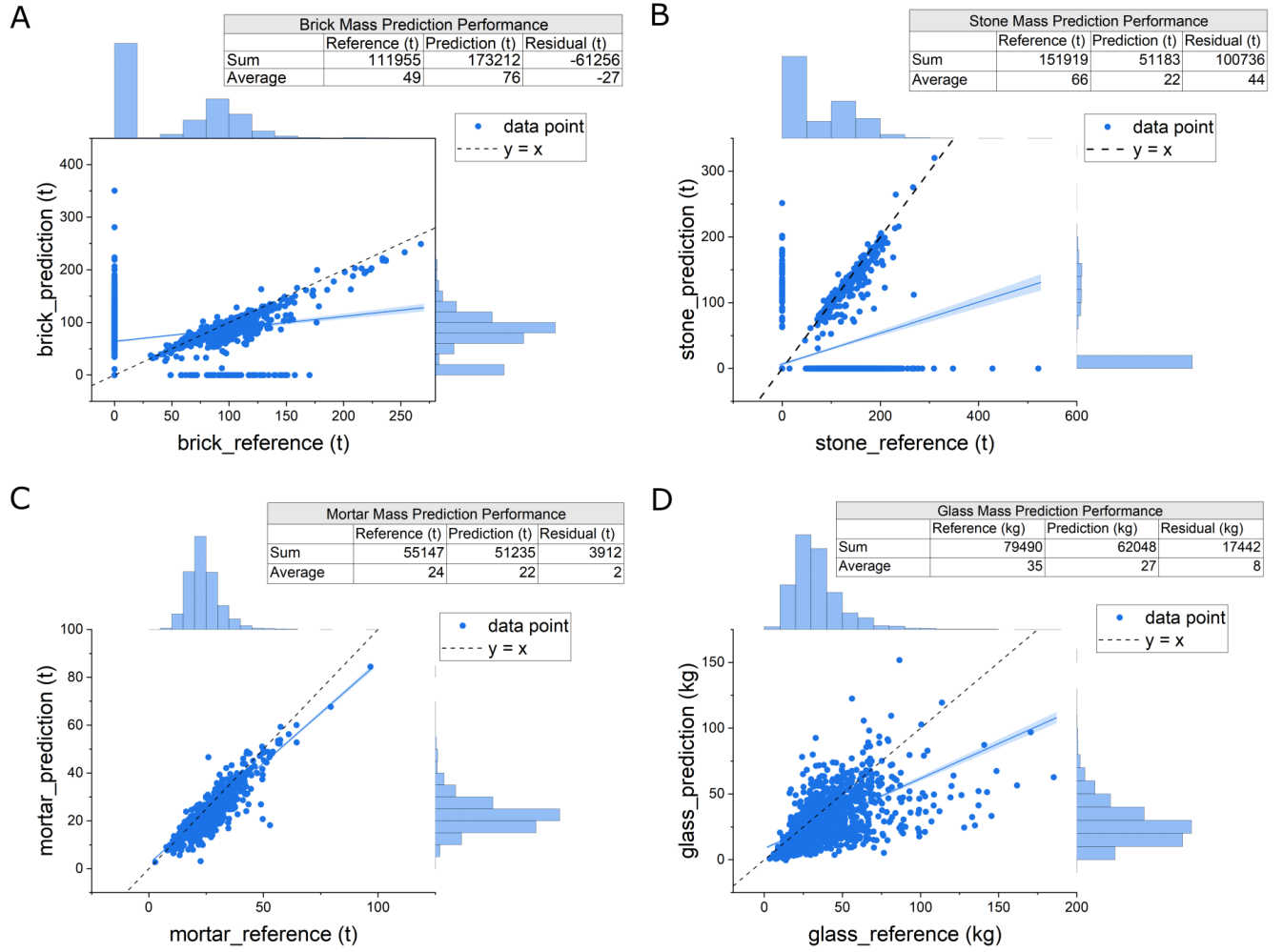


Figure 3: The mass prediction performance results for each material type. The reference values indicate the masses calculated by using EPC data and manually measured variables. The prediction values are produced by using the proposed computer vision-based mass estimation approach. For each material type, their linear regression fitting with a 95% confidence interval is calculated and another line with gradient being one is also presented. The total and average masses of each material and residuals of reference and prediction values are recorded in the top-right table of each figure.

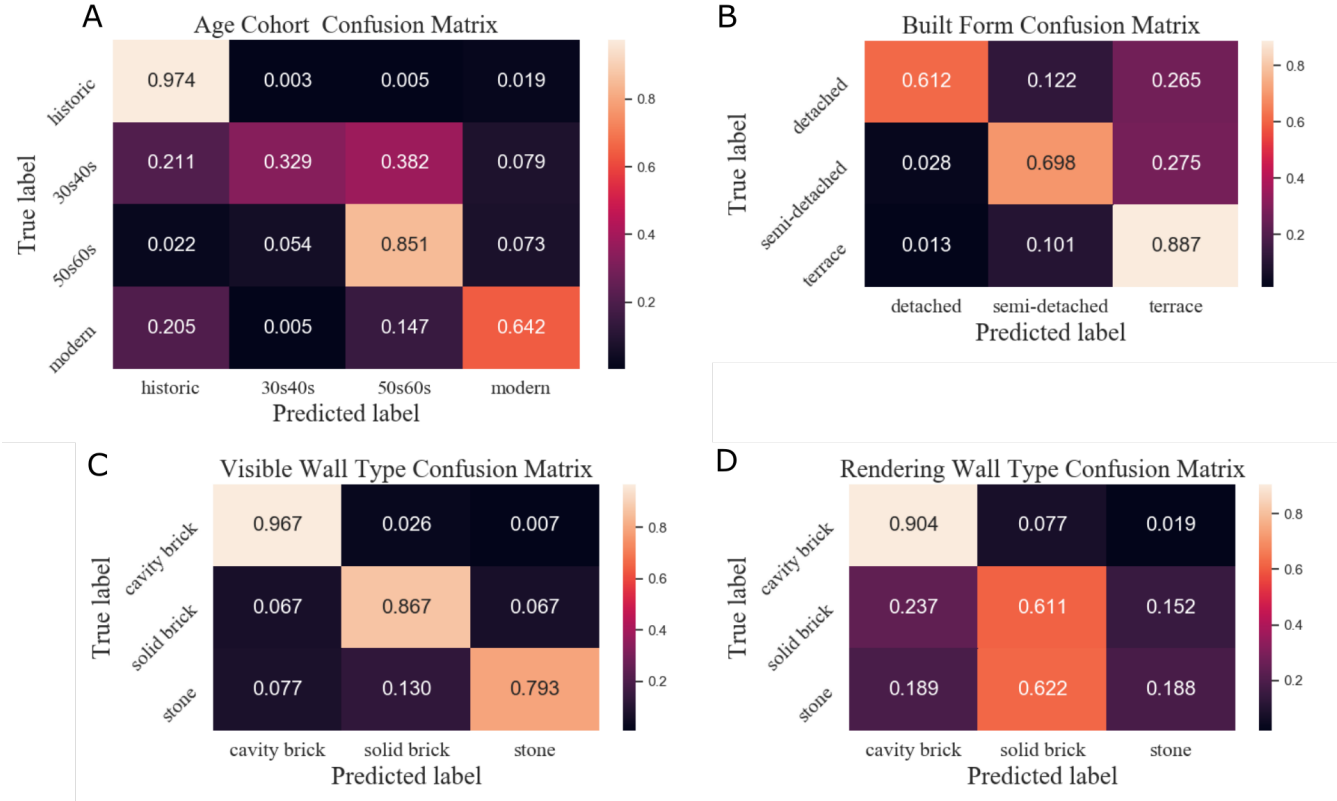


Figure 4: The results of the deployment of the age cohort (as seen in Subfigure A), built form (Subfigure B), and wall type predictions are presented. Due to the inability to directly predict the wall types of rendering walls, the prediction performance is assessed separately. Subfigure C pertains to buildings with visible wall materials, while Subfigure D relates to those with rendering walls.

384 **Age cohort prediction** The model achieved a 90% accuracy on the deployment dataset.
385 As illustrated in Figure 4-A, the model exhibited superior performance for historic (97.4%)
386 and 50s60s (85.1%) buildings but was less effective in identifying modern (64.2%) and 30s40s
387 (32.9%) structures. Although the overall accuracy on the deployment data surpassed the
388 validation results (90% versus 86%), the model underperformed in classifying modern (64.2%
389 compared to 76.5%) and 30s40s (32.9% versus 49.1%) buildings. Notably, the deployment
390 data indicated confusion between modern and historic buildings, a trend absent in the val-
391 idation dataset. The 30s40s category consistently displayed significant misclassifications
392 towards neighbouring age groups in both datasets.

393 **Built form prediction** On the deployment dataset, the built form prediction attained
394 an overall accuracy of 85% similar to the validation set (88%). As depicted in Figure 4-B,
395 the model demonstrated reduced efficacy in classifying semi-detached (69.8%) and detached
396 (61.2%) buildings. This trend was also observed in the validation dataset, though the per-
397 formance was superior—77.4% for semi-detached and 70.6% for detached buildings.

398 **Wall type prediction** Figure 4-C and D present the performances of wall type predictions.
399 Distinct evaluations are conducted for visible walls and rendered walls, given the latter's
400 predictions hinge on assumptions and age cohort determinations. For visible walls, the model
401 excelled with an overall accuracy of 90%, achieving 96.7% for cavity walls, 86.7% for solid
402 brick walls, and 79.3% for stone walls. Conversely, rendered wall predictions in Figure 4-
403 D indicate that solid walls are often misclassified as cavity brick or stone. Notably, stone
404 predictions frequently coincide with solid bricks due to the assignment of rendered walls in
405 historic buildings to solid brick types, leading to the potential overlooking of rendered stone
406 walls.

407 **Segmentation and Inner Wall Regression Models** Figure 5 demonstrates the quan-
408 titative performance of the proposed FacMagNet-s model. The wall and window predictions

Table 1: The inner wall regression results. Ten different random states have been tested on the built dataset. Four evaluation metrics are selected to evaluate the model performance.

Seed	Avg.	1	6	22	31	38	48	72	93	98
R^2	0.81	0.82	0.81	0.80	0.85	0.83	0.81	0.81	0.80	0.79
MAE	2.67	2.48	2.68	2.97	2.69	2.49	2.51	2.89	2.73	2.75
MSE	12.00	10.09	13.10	14.07	12.19	10.91	10.55	13.58	12.86	12.64
RMSE	3.46	3.18	3.62	3.75	3.49	3.30	3.25	3.68	3.59	3.56

409 have achieved 91.4% and 91.1% in pixel accuracy, respectively which lays a robust founda-
410 tion for window distribution and glass mass estimation.

411

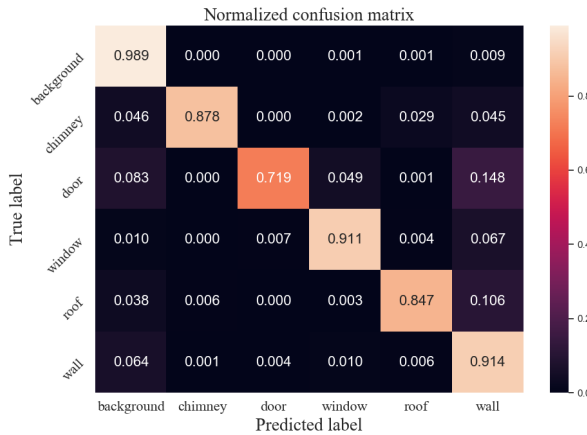


Figure 5: The confusion matrix of the proposed facade segmentation model.

412 Meanwhile, Table 1 presents an evaluation of the Multi-Layer Perceptron (MLP) algo-
413 rithm's performance for the task of inner wall regression. To ascertain model robustness,
414 ten distinct random state seeds are assessed. Overall, the MLP model attains an R^2 score of
415 0.81, signifying a pronounced correlation between the chosen independent variables and the
416 dependent variable, namely, the inner wall length. With a mean inner wall length computed
417 at 30.75m, the RMSE suggests an average prediction error margin of 11%.

418

419 **Facade Information-based Building Material Stock Estimation**

420 Factors influencing mass prediction accuracy fall into two categories: dimensional and clas-
421 sification. Dimensional inaccuracies encompass errors in predicting building footprint and
422 window size, while classification errors arise from the performance of trained models. No-
423 tably, errors in predicting wall types have a significant bearing on estimating brick and stone
424 masses, as illustrated in Figure 3.

425

426 Figure 4-C and D reveal that visible walls exhibit markedly superior accuracy for solid
427 brick and stone than rendered walls. This underscores that the presence of rendered walls
428 primarily constrains precise estimations. When samples with incorrect wall type predic-
429 tions are excluded, brick and stone mass prediction errors stand at 8% and 7% respec-
430 tively—substantially lower than the overarching error rates of 55% and 67%. Such findings,
431 along with the mortar mass prediction results, suggest that dimensional errors have minimal
432 impact. This supports the efficacy of employing the Douglas-Peuker algorithm and bounding
433 boxes for estimating floorplan dimensions.

434

435 Glass mass predictions hinge on the accuracy of window dimension predictions, which
436 in turn are greatly influenced by facade segmentation quality. The number of wall pixels
437 dictates image resolution, and the precision of window recognition further affects these esti-
438 mations. Additionally, inconsistencies in age cohort predictions sway glass mass predictions
439 given their role in specifying glazing types.

440

441 In summation, the data affirms the viability of utilising facade images and computer
442 vision methods to gauge building material stock, particularly for visible wall types. The
443 methodology, however, demonstrates limitations in predicting the mass of rendered wall
444 buildings, especially for stone.

445 The Reference Level Uncertainties and Approach Limitations

446 In this research, the reference level is derived from EPC records coupled with manually mea-
447 sured dimensions. However, given that EPC records are based on onsite evaluations, they
448 inherently possess inaccuracies⁶⁴. This makes the difference between the calculated reference
449 level and the ground truth uncertain. A study by Hardy et al. (2019)⁶⁴ assessed the precision
450 of EPC records and found that 27% of them contained discrepancies, with approximately
451 11% of buildings exhibiting wall types inconsistent with their records.

452

453 Our team manually labelled the housing attribute dataset based on their visual wall
454 types. Findings reveal that the accuracy stands at 90.8% for cavity brick, 86.7% for solid
455 brick, and 91.3% for stone walls. Consequently, the exact error rate for rendered walls is
456 indeterminate. Moreover, from our observations, a subset of rendered wall buildings appear
457 more akin to brick than stone walls, intensifying the challenge of accurately ascertaining the
458 true wall types for rendered walls.

459

460 The results for the inner wall length regression demonstrate inherent uncertainties. The
461 benchmark for inner wall length derives from EPC records complemented by manual mea-
462 surements. Nonetheless, the model imparts an error margin of $\pm 11\%$, thus making the
463 benchmark somewhat indeterminate. Additionally, while the predicted inner walls are pre-
464 sumed to be constructed from structural materials, i.e. brick or stone, the prevalence of
465 plasterboard as partition walls in contemporary homes cannot be overlooked. Though ef-
466 forts were made to exclude evident plasterboard partition walls during dataset annotation,
467 the exact nature of the inner walls remains ambiguous without a comprehensive onsite survey.

468

469 Additionally, our assumptions consider only brick and stone as construction materials.
470 Yet, some houses may be constructed using concrete blocks. Given that EPC records lack
471 detailed descriptions concerning concrete blocks, and visually determining a building's con-

⁴⁷² struction as concrete-based is inherently challenging, the incorporation of concrete remains
⁴⁷³ ambiguous.

⁴⁷⁴ **The Path Towards an Efficient Component-Level Building Material Stock Future**

⁴⁷⁶ A fundamental limitation of contemporary methods for estimating building material stock
⁴⁷⁷ is resolution. Typical strategies, such as employing optical remote sensing or nighttime light
⁴⁷⁸ images, fail to achieve component-level material estimation. Conversely, traditional bottom-
⁴⁷⁹ up accounting necessitates labour-intensive onsite surveys.

⁴⁸⁰

⁴⁸¹ Drive-by facade images offer a cost-effective and efficient avenue for obtaining building
⁴⁸² attributes. Our research underscores that, with the aid of computer vision techniques, build-
⁴⁸³ ing attributes crucial for stock estimation can be reliably discerned, except in the case of
⁴⁸⁴ buildings with rendering walls. While this approach mandates the use of building footprint
⁴⁸⁵ data, the increasing ubiquity of built environment research renders this data readily accessi-
⁴⁸⁶ ble.^{65,66} As such, the method developed and presented in this paper signifies a step towards
⁴⁸⁷ a streamlined component-level mass estimation.

⁴⁸⁸

⁴⁸⁹ Moving forward, our primary objectives are to address the current method's limitations:
⁴⁹⁰ particularly concrete estimation, rendered wall construction material prediction, and the
⁴⁹¹ exclusion of plasterboard. Given the constraints of computer vision techniques, only visi-
⁴⁹² ble attributes can be captured. Nevertheless, buildings, as rigorously regulated constructs,
⁴⁹³ possess attributes that might be deduced using age cohort data. For instance, the popu-
⁴⁹⁴ larity of concrete buildings and plasterboard surged post-World War II, attributed to their
⁴⁹⁵ cost-effectiveness and ease of installation. Encoding building regulations into our approach
⁴⁹⁶ promises a more holistic and precise trajectory for component-level building mass estimation.

⁴⁹⁷

498 Overall, building stock, a critical component of the built environment, serves as a repos-
499 itory of readily available and recoverable materials, effectively acting as an "above-ground
500 mine". The foundation of a circular economy lies in the perpetuation of a materials loop,
501 which strives to diminish and ultimately negate the need for extracting virgin resources.
502 Precise knowledge of building materials at the component level allows for an accurate as-
503 sessment of secondary resources and the forecasting of material demand. This granularity in
504 accounting for building stock is indispensable, not only for tapping into the vast potential
505 of material reuse but also for propelling the full scope of product recovery necessary for a
506 thriving circular economy.

507 Data and Code Availability

508 Due to privacy constraints, image data from the vehicle-mounted capture platform will
509 remain inaccessible to the public. However, the Google Street View data employed for model
510 training is retrievable through the Street View API. Upon this paper's publication, the query
511 locations—encompassing both location details and labels from their EPC records—the inner
512 wall regression dataset, the building attributes dataset, and developed software packages will
513 be made available on the designated GitHub repository: https://github.com/MerlinDai/MARVEL_StockQuantification.

515 Author Contributions

516 **Menglin Dai:** Conceptualisation, Methodology, Software, Validation, Investigation, Data
517 Curation, Formal analysis, Writing - Original Draft, Writing - Review & Editing, Visualisa-
518 tion **Jakub Jurczyk:** Methodology, Validation, Data Curation **Hadi Arbabi:** Writing -
519 Review & Editing **Ruichang Mao:** Writing - Review & Editing **Wil Ward:** Data Cura-
520 tion **Martin Mayfield:** Resources, Funding acquisition **Gang Liu:** Supervision, Writing
521 - Review & Editing **Danielle Densley Tingley:** Conceptualisation, Resources, Project
522 administration, Funding acquisition, Supervision, Writing - Review & Editing

523 Acknowledgement

524 This work was supported by EPSRC Active Building Centre Research Programme, United
525 Kingdom [EP/V012053/1] and EPSRC Multi-Scale, Circular Economic Potential of Non-
526 Residential Building Scale [EP/S029273/1].

⁵²⁷ **Supporting Information Available**

⁵²⁸ The following files are available free of charge.

- ⁵²⁹ • supplementary_file.pdf: This file contains additional details of built datasets and de-
⁵³⁰ veloped machine learning models.

531 **References**

- 532 (1) International Energy Agency *Tracking Clean Energy Progress 2023*; 2023; License: CC
533 BY 4.0.
- 534 (2) United Nations Sustainable Development Goals. 2015; <https://www.un.org/sustainabledevelopment/sustainable-development-goals/> (accessed 2023-06-
535 06).
- 536 (3) Elhacham, E.; Ben-Uri, L.; Grozovski, J.; Bar-On, Y. M.; Milo, R. Global human-made
537 mass exceeds all living biomass. *Nature* **2020**, *588*, 442–444.
- 538 (4) Krausmann, F.; Wiedenhofer, D.; Lauk, C.; Haas, W.; Tanikawa, H.; Fishman, T.;
539 Miatto, A.; Schandl, H.; Haberl, H. Global socioeconomic material stocks rise 23-fold
540 over the 20th century and require half of annual resource use. *Proceedings of the National
541 Academy of Sciences* **2017**, *114*, 1880–1885.
- 542 (5) Densley Tingley, D. Embed circular economy thinking into building retrofit. *Communications
543 Engineering* **2022**, *1*, 1–4.
- 544 (6) Koutamanis, A.; van Reijn, B.; van Bueren, E. Urban mining and buildings: A review of
545 possibilities and limitations. *Resources, Conservation and Recycling* **2018**, *138*, 32–39.
- 546 (7) Wiedenhofer, D.; Steinberger, J. K.; Eisenmenger, N.; Haas, W. Maintenance and ex-
547 pansion: modeling material stocks and flows for residential buildings and transportation
548 networks in the EU25. *Journal of Industrial Ecology* **2015**, *19*, 538–551.
- 549 (8) Lanau, M.; Liu, G.; Kral, U.; Wiedenhofer, D.; Keijzer, E.; Yu, C.; Ehlert, C. Taking
550 stock of built environment stock studies: Progress and prospects. *Environmental science
551 & technology* **2019**, *53*, 8499–8515.
- 552 (9) Li, Q.; Gummidi, S. R. B.; Lanau, M.; Yu, B.; Liu, G. Spatiotemporally Explicit
553 Mapping of Built Environment Stocks Reveals Two Centuries of Urban Development

- 555 in a Fairytale City, Odense, Denmark. *Environmental Science & Technology* **2022**, *56*,
556 16369–16381.
- 557 (10) Augiseau, V.; Barles, S. Studying construction materials flows and stock: A review.
558 *Resources, Conservation and Recycling* **2017**, *123*, 153–164.
- 559 (11) Mohammadiziazi, R.; Bilec, M. Building material stock analysis is critical for effective
560 circular economy strategies: a comprehensive review. *Environmental Research: Infrastruc-*
561 *ture and Sustainability* **2022**, *2*, 032001.
- 562 (12) Shi, F.; Huang, T.; Tanikawa, H.; Han, J.; Hashimoto, S.; Moriguchi, Y. Toward a low
563 carbon–dematerialization society: Measuring the materials demand and CO₂ emissions
564 of building and transport infrastructure construction in China. *Journal of Industrial*
565 *Ecology* **2012**, *16*, 493–505.
- 566 (13) Huang, T.; Shi, F.; Tanikawa, H.; Fei, J.; Han, J. Materials demand and environmental
567 impact of buildings construction and demolition in China based on dynamic material
568 flow analysis. *Resources, Conservation and Recycling* **2013**, *72*, 91–101.
- 569 (14) Fishman, T.; Schandl, H.; Tanikawa, H.; Walker, P.; Krausmann, F. Accounting for the
570 material stock of nations. *Journal of Industrial Ecology* **2014**, *18*, 407–420.
- 571 (15) Gao, X.; Nakatani, J.; Zhang, Q.; Huang, B.; Wang, T.; Moriguchi, Y. Dynamic ma-
572 terial flow and stock analysis of residential buildings by integrating rural–urban land
573 transition: A case of Shanghai. *Journal of Cleaner Production* **2020**, *253*, 119941.
- 574 (16) Nasir, U.; Chang, R.; Omrany, H. Calculation methods for construction material stocks:
575 A systematic review. *Applied Sciences* **2021**, *11*, 6612.
- 576 (17) Tanikawa, H.; Hashimoto, S. Urban stock over time: spatial material stock analysis
577 using 4d-GIS. *Building research & information* **2009**, *37*, 483–502.

- 578 (18) Ortlepp, R.; Gruhler, K.; Schiller, G. Material stocks in Germany's non-domestic build-
579 ings: a new quantification method. *Building Research & Information* **2016**, *44*, 840–
580 862.
- 581 (19) Heeren, N.; Fishman, T. A database seed for a community-driven material intensity
582 research platform. *Scientific data* **2019**, *6*, 23.
- 583 (20) Mao, R.; Bao, Y.; Huang, Z.; Liu, Q.; Liu, G. High-resolution mapping of the urban
584 built environment stocks in Beijing. *Environmental science & technology* **2020**, *54*,
585 5345–5355.
- 586 (21) Lanau, M.; Liu, G. Developing an urban resource cadaster for circular economy: A case
587 of Odense, Denmark. *Environmental science & technology* **2020**, *54*, 4675–4685.
- 588 (22) Sprecher, B.; Verhagen, T. J.; Sauer, M. L.; Baars, M.; Heintz, J.; Fishman, T. Material
589 intensity database for the Dutch building stock: Towards Big Data in material stock
590 analysis. *Journal of Industrial Ecology* **2022**, *26*, 272–280.
- 591 (23) Haberl, H.; Wiedenhofer, D.; Schug, F.; Frantz, D.; Virág, D.; Plutzar, C.; Gruhler, K.;
592 Lederer, J.; Schiller, G.; Fishman, T.; others High-resolution maps of material stocks
593 in buildings and infrastructures in Austria and Germany. *Environmental science &
594 technology* **2021**, *55*, 3368–3379.
- 595 (24) Bao, Y.; Huang, Z.; Wang, H.; Yin, G.; Zhou, X.; Gao, Y. High-resolution quantification
596 of building stock using multi-source remote sensing imagery and deep learning. *Journal
597 of Industrial Ecology* **2023**, *27*, 350–361.
- 598 (25) Liu, Z.; Saito, R.; Guo, J.; Hirai, C.; Haga, C.; Matsui, T.; Shirakawa, H.; Tanikawa, H.
599 Does Deep Learning Enhance the Estimation for Spatially Explicit Built Environment
600 Stocks through Nighttime Light Data Set? Evidence from Japanese Metropolitans.
601 *Environmental Science & Technology* **2023**, *57*, 3971–3979.

- 602 (26) Arbabi, H.; Lanau, M.; Li, X.; Meyers, G.; Dai, M.; Mayfield, M.; Densley Tingley, D. A
603 scalable data collection, characterization, and accounting framework for urban material
604 stocks. *Journal of Industrial Ecology* **2022**, *26*, 58–71.
- 605 (27) Francart, N.; Gummidi, S.; Hoxha, E.; Birgisdottir, H. A Danish model of building
606 macro-components to promote circularity. *Journal of Physics: Conference Series*. 2023;
607 p 192001.
- 608 (28) Shen, L.; Yang, Q.; Yan, H. Spatial Characterization Analysis of Residential Material
609 Stock and its Driving Factors: A Case Study of Xi'an. *Buildings* **2023**, *13*, 581.
- 610 (29) Anguelov, D.; Dulong, C.; Filip, D.; Frueh, C.; Lafon, S.; Lyon, R.; Ogale, A.; Vin-
611 cent, L.; Weaver, J. Google Street View: Capturing the World at Street Level. *Computer*
612 **2010**, *43*, 32–38.
- 613 (30) Biljecki, F.; Ito, K. Street view imagery in urban analytics and GIS: A review. *Landscape*
614 and *Urban Planning* **2021**, *215*, 104217.
- 615 (31) Kang, J.; Körner, M.; Wang, Y.; Taubenböck, H.; Zhu, X. X. Building instance classifi-
616 cation using street view images. *ISPRS journal of photogrammetry and remote sensing*
617 **2018**, *145*, 44–59.
- 618 (32) Zeppelzauer, M.; Despotovic, M.; Sakeena, M.; Koch, D.; Döller, M. Automatic predic-
619 tion of building age from photographs. *Proceedings of the 2018 ACM on International*
620 *Conference on Multimedia Retrieval*. 2018; pp 126–134.
- 621 (33) Szcześniak, J. T.; Ang, Y. Q.; Letellier-Duchesne, S.; Reinhart, C. F. A method for
622 using street view imagery to auto-extract window-to-wall ratios and its relevance for
623 urban-level daylighting and energy simulations. *Building and Environment* **2022**, *207*,
624 108108.

- 625 (34) Ministry of Housing, Communities & Local Government English Housing Survey,
626 Households Report, 2017-18. 2018; [https://www.gov.uk/government/statistics/
627 english-housing-survey-2017-to-2018-households](https://www.gov.uk/government/statistics/english-housing-survey-2017-to-2018-households) (accessed 2023-06-06).
- 628 (35) Dai, M.; Ward, W. O.; Arbabi, H.; Densley Tingley, D.; Mayfield, M. Scalable Res-
629 idential Building Geometry Characterisation Using Vehicle-Mounted Camera System.
630 *Energies* **2022**, *15*, 6090.
- 631 (36) Loga, T.; Stein, B.; Diefenbach, N. TABULA building typologies in 20 European coun-
632 tries—Making energy-related features of residential building stocks comparable. *Energy
633 and Buildings* **2016**, *132*, 4–12.
- 634 (37) Meyers, G.; Zhu, C.; Mayfield, M.; Tingley, D. D.; Willmott, J.; Coca, D. Design-
635 ing a Vehicle Mounted High Resolution Multi-Spectral 3D Scanner: Concept Design.
636 Proceedings of the 2nd Workshop on Data Acquisition to Analysis. 2019; pp 16–21.
- 637 (38) Ward, W.; Dai, M.; Arbabi, H.; Sun, Y.; Tingley, D.; Mayfield, M. Measuring the
638 Cityscape: A Pipeline from Street-Level Capture to Urban Quantification. *IOP Con-
639 ference Series: Earth and Environmental Science* **2022**, *1078*, 012036.
- 640 (39) Ward, W.; Li, X.; Sun, Y.; Dai, M.; Arbabi, H.; Tingley, D. D.; Mayfield, M. Estimat-
641 ing energy consumption of residential buildings at scale with drive-by image capture.
642 *Building and Environment* **2023**, *234*, 110188.
- 643 (40) Ordnance Survey MasterMap topography layer. 2023; [https://www.ordnancesurvey.
644 co.uk/business-government/products/mastermap-topography](https://www.ordnancesurvey.co.uk/business-government/products/mastermap-topography) (accessed 2023-05-
645 15).
- 646 (41) A flexible new technique for camera calibration. *IEEE Transactions on pattern analysis
647 and machine intelligence* **2000**, *22*, 1330–1334.

- 648 (42) Cucchiara, R.; Grana, C.; Prati, A.; Vezzani, R. A Hough transform-based method for
649 radial lens distortion correction. 12th International Conference on Image Analysis and
650 Processing, 2003. Proceedings. 2003; pp 182–187.
- 651 (43) BPIE Energy Performance Certificates across the EU. 2015.
- 652 (44) Piddington, J.; Nicol, S.; Garrett, H.; Custard, M. The Housing Stock of the United
653 Kingdom. *BRE Trust: Watford, UK* **2020**, https://files.bregroup.com/bretrust/The-Housing-Stock-of-the-United-Kingdom_Report_BRE-Trust.pdf (accessed
654 2023-06-06).
- 655 (45) Dai, M.; Ward, W. O.; Meyers, G.; Tingley, D. D.; Mayfield, M. Residential building
656 facade segmentation in the urban environment. *Building and Environment* **2021**, *199*,
657 107921.
- 658 (46) Sun, M.; Zhang, F.; Duarte, F.; Ratti, C. Understanding architecture age and style
659 through deep learning. *Cities* **2022**, *128*, 103787.
- 660 (47) Benz, A.; Voelker, C.; Daubert, S.; Rodehorst, V. Towards an automated image-based
661 estimation of building age as input for Building Energy Modeling (BEM). *Energy and
662 Buildings* **2023**, *292*, 113166.
- 663 (48) Wei, X.-S.; Song, Y.-Z.; Mac Aodha, O.; Wu, J.; Peng, Y.; Tang, J.; Yang, J.; Be-
664 longie, S. Fine-grained image analysis with deep learning: A survey. *IEEE transactions
665 on pattern analysis and machine intelligence* **2021**, *44*, 8927–8948.
- 666 (49) Lin, T.-Y.; RoyChowdhury, A.; Maji, S. Bilinear CNN models for fine-grained visual
667 recognition. Proceedings of the IEEE international conference on computer vision. 2015;
668 pp 1449–1457.
- 669 (50) Meng, C.; Song, Y.; Ji, J.; Jia, Z.; Zhou, Z.; Gao, P.; Liu, S. Automatic classification
670

- of rural building characteristics using deep learning methods on oblique photography. *Building Simulation*. 2022; pp 1–14.
- (51) He, K.; Zhang, X.; Ren, S.; Sun, J. Deep Residual Learning for Image Recognition. Proceedings of the IEEE Conference on Computer Vision and Pattern Recognition. 2016; pp 770–778.
- (52) Chollet, F. Xception: Deep learning with depthwise separable convolutions. Proceedings of the IEEE conference on computer vision and pattern recognition. 2017; pp 1251–1258.
- (53) Martinovic, A.; Knopp, J.; Riemenschneider, H.; Van Gool, L. 3d all the way: Semantic segmentation of urban scenes from start to end in 3d. Proceedings of the IEEE Conference on Computer Vision and Pattern Recognition. 2015; pp 4456–4465.
- (54) Gadde, R.; Jampani, V.; Marlet, R.; Gehler, P. V. Efficient 2D and 3D Facade Segmentation Using Auto-Context. *IEEE Transactions on Pattern Analysis and Machine Intelligence* **2017**, *40*, 1273–1280.
- (55) Kong, G.; Fan, H. Enhanced Facade Parsing for Street-Level Images Using Convolutional Neural Networks. *IEEE Transactions on Geoscience and Remote Sensing* **2020**, *59*, 10519–10531.
- (56) Zhang, G.; Pan, Y.; Zhang, L. Deep learning for detecting building façade elements from images considering prior knowledge. *Automation in Construction* **2022**, *133*, 104016.
- (57) Chen, L.-C.; Zhu, Y.; Papandreou, G.; Schroff, F.; Adam, H. Encoder-Decoder with Atrous Separable Convolution for Semantic Image Segmentation. Proceedings of the European Conference on Computer Vision (ECCV). 2018; pp 833–851.
- (58) Watson, P. An introduction to UK energy performance certificates (EPCs). *Journal of Building Appraisal* **2010**, *5*, 241–250.

- 694 (59) Fewins, C. The pros and cons of different construction systems. *Home Building &*
695 *Renovating* **2004**, 1–11.
- 696 (60) Yuan, L.; Lu, W.; Xue, F.; Li, M. Building feature-based machine learning regression
697 to quantify urban material stocks: A Hong Kong study. *Journal of Industrial Ecology*
698 **2023**, 27, 336–349.
- 699 (61) Pedregosa, F.; Varoquaux, G.; Gramfort, A.; Michel, V.; Thirion, B.; Grisel, O.; Blon-
700 del, M.; Prettenhofer, P.; Weiss, R.; Dubourg, V.; others Scikit-learn: Machine learning
701 in Python. *the Journal of Machine Learning research* **2011**, 12, 2825–2830.
- 702 (62) Summers, C.; Hulme, J. *BRE Client Report for EPISCOPE Pilot Project: Eng-*
703 *land, Intelligent Energy Europe Programme for the European Union; Client*
704 *Report 297809, 2016;* https://episcope.eu/fileadmin/episcope/public/docs/pilot_actions/GB_EPISCOPE_NationalCaseStudy_BRE.pdf (accessed 2023-06-06).
- 706 (63) Institution, B. S. *BS EN 771-1 Specification for Masonry Units. Part 1: Clay Masonry*
707 *Units*; 2020.
- 708 (64) Hardy, A.; Glew, D. An analysis of errors in the Energy Performance certificate
709 database. *Energy policy* **2019**, 129, 1168–1178.
- 710 (65) Sirko, W.; Kashubin, S.; Ritter, M.; Annkah, A.; Bouchareb, Y. S. E.; Dauphin, Y.;
711 Keysers, D.; Neumann, M.; Cisse, M.; Quinn, J. Continental-scale building detection
712 from high resolution satellite imagery. **2021**, *arXiv preprint arXiv:2107.12283*, <https://arxiv.org/abs/2107.12283> (accessed 2023-06-06).
- 714 (66) Milojevic-Dupont, N.; Wagner, F.; Nachtigall, F.; Hu, J.; Brüser, G. B.; Zumwald, M.;
715 Biljecki, F.; Heeren, N.; Kaack, L. H.; Pichler, P.-P.; others EUBUCCO v0. 1: Euro-
716 pean building stock characteristics in a common and open database for 200+ million
717 individual buildings. *Scientific Data* **2023**, 10, 147.

718 TOC Graphic

719

